International Journal of Thermal Sciences 118 (2017) 12–23

Contents lists available at ScienceDirect

International Journal of Thermal Sciences

journal homepage: www.elsevier.com/locate/ijts

Using a magnetic field to reduce natural convection in a vertical cylindrical annulus

Masoud Afrand

Department of Mechanical Engineering, Najafabad Branch, Islamic Azad University, Najafabad, Iran

ARTICLE INFO

Article history:
Received 3 April 2016
Received in revised form
10 April 2017
Accepted 11 April 2017

Keywords:
Vertical cylindrical annulus
Nusselt number
Hartman number
Prandtl number
Induced electric field
Numerical simulation

ABSTRACT

This paper presents the investigation of laminar natural convection in 3D vertical cylindrical annulus containing electrically conductive fluids under a horizontal magnetic field. The model was composed of two isothermal coaxial cylinders. Both ends of the cylinders were supposed adiabatic and all walls were assumed electrically insulated. Complex nonlinear governing equations were solved numerically by means of the finite volume method. The effects of different parameters such as the strength of the magnetic field, the radii ratio, aspect ratio, and Prandtl number on the temperature distribution, average Nusselt number, distribution of Lorentz forces as well as induced electric field were investigated. Results showed that for aspect ratios lower than about 1, the average Nusselt number increased as aspect ratio was increased. When aspect ratio was greater than about 1, the average Nusselt number decreases as aspect ratio was enlarged. Moreover, results showed that the average Nusselt number increased as radii ratio was increased. Results also revealed that a stronger magnetic field was needed to achieve pure conduction in the case of thick annulus. The presence of magnetic field induced an electric field which affected the Lorentz force. Distributions of Lorentz force and induced electric field indicated respectively the formation of Hartmann and Roberts layers. Furthermore, the average Nusselt number increased with increasing Prandtl number at all Hartmann numbers. It was also found that with increasing Hartmann number, the effect of Prandtl number on the average Nusselt number decreased.

1. Introduction

Nowadays, magnetic fields are widely used in most important industries. In cooling or heating applications, increasing the heat transfer is considered by the magnetic field. For this purpose, researchers have also introduced magnetic nanofluids [1–7]. In some heat transfer applications, magnetic fields are for nuclear reactor cooling systems, pumping, stirring, and levitation of magnetic materials [8–11]. Magnetic fields also could be employed to attenuate the fluid flows caused by natural convection [12–14].

During crystal growth processes, the temperature gradient in the melt, which is due to the temperature difference between the solid wall of the container and the melt, causes Buoyancy forces in the melt. In most practical cases, the random and irregular motions caused by this effect lead to microscopic inhomogeneity of the manufactured materials. Hence, in such applications, reduction of convection heat transfer is of great interest. As mentioned above, the use of magnetic fields is an effective method to reduce this type of heat transfer in electrically conducting fluids. Since the interactions between the magnetic field and the fluid flow cause Lorentz forces, which always oppose the direction of fluid motion. Nonetheless, the magnetic fields can also cause electric potential, which counteracts the Lorentz forces. Hence, the induced electric potential can negatively affect the desired objectives of the magnetic field [15,16].

Since magnetic control of fluid flows in annulus can be used in different applications, the convection heat transfer in fluids subject to magnetic fields has been intensely studied. For instance, Mozayyenin and Rahimi [17] numerically investigated the mixed convection heat transfer in cylindrical annulus of constant wall temperature subject to a radial magnetic field. Different combination of dimensionless numbers including Reynolds number, Hartmann number, Rayleigh number, Eckert number, and the ratio of the annulus gap width was considered in their study. Their numerical results indicated that the fluid flow and heat transfer were significantly suppressed by applying the magnetic field. Teimouri et al. [18] numerically studied free convection in a long horizontal

E-mail addresses: masoud.afrand@pmc.iaun.ac.ir, masoud_afrand@yahoo.com.

http://dx.doi.org/10.1016/j.ijthermalsci.2017.04.012
1290-0729/

Nomenclature

A	aspect ratio
B	magnitude of the external magnetic field (kg/s^2A)
D	annulus gap $(D = r_o - r_i(m))$
E	dimensional induced electric field (mkg/s^3A)
E^*	dimensionless induced electric field
F	Lorentz force (N/m^3)
F^*	dimensionless Lorentz force
g	acceleration due to gravity (m/s^2)
H	height of the annulus
Ha	Hartmann number
J	electric current density (A/m^2)
n	normal vector (m)
Nu	Nusselt number
p	pressure (N/m^2)
P	dimensionless pressure
Pr	Prandtl number
Ra	Rayleigh number
T	dimensional temperature (K)
T^*	dimensionless temperature
(r, z)	radial and axial co-ordinates
(R, Z)	dimensionless radial and axial co-ordinates
(r_i, r_o)	radii of inner and outer cylinders (m)
(u, v, w)	dimensional velocity components in (r, θ, z) direction (m/s)
(U, V, W)	dimensionless velocity components in (r, θ, z) direction
(x, y, z)	Cartesian co-ordinate components

Greek letters

α	thermal diffusivity (m^2/s)
β	fluid coefficient of thermal expansion $(1/K)$
φ	dimensional electrical potential (m^2kg/s^3A)
Φ	dimensionless electrical potential
γ	inclination angle
λ	radii ratio
μ	dynamic viscosity (kg/ms)
θ	azimuthal angle
ρ	fluid density (kg/m^3)
σ	fluid electrical conductivity (s^3A^2/m^3kg)

Subscripts

c	condition at cold wall
h	condition at hot wall
i	inner cylinder
o	outer cylinder

cylindrical annulus filled with molten potassium exposed to a radial magnetic field. Their results revealed that with increasing radii ratio, the influence of magnetic field on free convection decreased. Sankar et al. [19] studied the effect of magnetic field on natural convection between two vertical concentric cylinders. Their study was performed on electrically conducting fluid with Prandtl numbers of 0.054 subject to axial and radial magnetic fields of constant strength. The temperatures of the inner and outer cylinders were kept constant. They used numerical approaches and demonstrated the effect of Rayleigh and Hartmann numbers on the isotherms and streamlines. Their results also indicated that in shallow annuluses the natural convection was repressed more effectively by an axial magnetic field, while in tall annuluses a radial magnetic field is more impressive. Wrobel et al. [20] conducted experimental and numerical studies on the fluid flow and heat transfer of a paramagnetic fluid between two vertical cylinders subject to a magnetic field. They concluded that the effect of Hartmann number on heat transfer was four times stronger than that of the Rayleigh number. Kabier et al. [21] analytically studied the heat and mass transfer in an impenetrable horizontal cylinder containing a non-Newtonian fluid in a porous media. The studied cavity was subject to a horizontal magnetic field. Many assumptions were made in their work, and the effect of different parameters including the strength of the magnetic field was investigated. Venkatachalappa et al. [22] studied the effect of radial and axial magnetic field on convection heat transfer and mass transfer in a hollow vertical cylinder using numerical methods. They demonstrated the effect of Hartmann number on isotherms as well as streamlines when subjected to radial or axial magnetic fields. Kumar and Singh [23] investigated the effect of radial magnetic field on laminar natural convective a viscous electrically conducting fluid between two concentric vertical cylinders. They observed that the fluid velocity and induced magnetic field were reduced with augmenting Hartmann number. Their results showed that this decreasing was more when one of the cylinders is conducting compared to when both cylinders are non-conducting. Kakarantzas et al. [15] studied the unsteady state effect of a constant horizontal magnetic field on a specific vertical annulus (with specific dimensions), and demonstrated the effect of magnetic field on isotherms and velocity. Numerical methods were used in their studies, and the Prandtl Number of the modeled fluid was 0.0321. According to their results, applying a magnetic field causes an electrical field, eliminating symmetry in the tangential direction. Afrand et al. [24] numerically investigated natural convection of electrically conducting fluid in an inclined cylindrical annulus under various magnetic fields. Their results revealed that the effect of transverse magnetic field on the average Nusselt number is more effective than that of the axial magnetic field. Further, Afrand et al. [25] performed 3D numerical simulation of natural convection of molten potassium in an inclined cylindrical annulus exposed to a magnetic field. They reported that a magnetic field can control the natural convection of molten potassium. Their results also revealed that the direction and strength of the magnetic field could have different effects on the suppression of natural convection. They also observed that increasing the strength of the magnetic field caused the loss symmetry.

According to the literature review, most studies have been conducted to examine the conditions that the induced electric potential caused by the magnetic field was not created or considered. Moreover, the effect of different parameters on various aspects of heat transfer and fluid flow in a vertical annulus under magnetic field were investigated, while their effects on the distribution of Lorentz forces and the induced electric potential were not considered. Hence, in the present study, the effect of different parameters such as the strength of the magnetic field, the radii ratio, length of annulus, and Prandtl number on the temperature distribution, distribution of Lorentz forces as well as induced electric field is investigated.

2. Mathematical formulation

In the present study, laminar natural convection heat transfer in 3-dimensional vertical cylindrical annuluses containing an electrically conductive fluid is investigated. The studied annulus are composed of cylinders with inner and outer radii as well as height of r_i, r_o, and H, respectively, as illustrated in Fig. 1. Since numerous

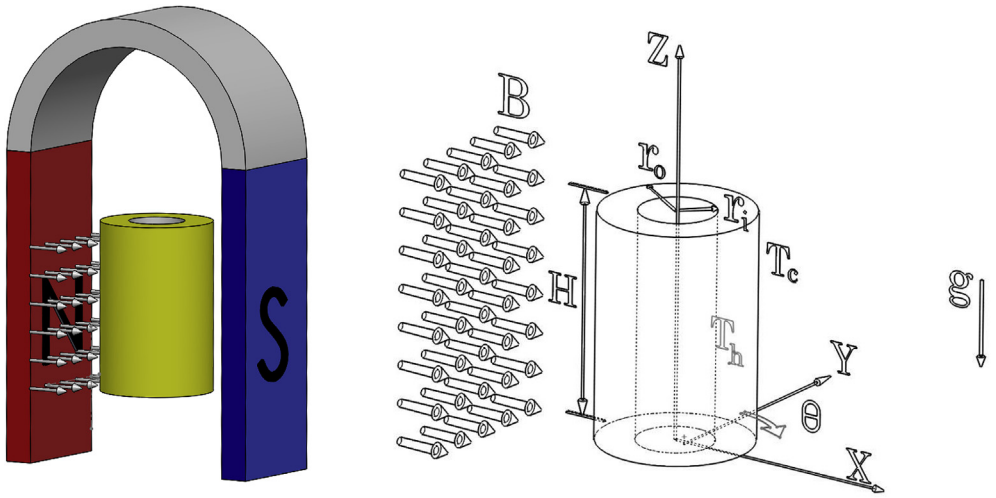

Fig. 1. Schematic of the present model.

studies in the literature have addressed the effect of Rayleigh number on heat transfer, the present study was conducted using a fixed value of Rayleigh number ($Ra = 10^5$). The boundary conditions in our study included constant temperatures of the inner and outer walls, represented by T_h and T_c, respectively, such that $T_c < T_h$, as well as two base walls of the annuluses with adiabatic conditions. Moreover, it was assumed that all walls are electrically insulated. In Fig. 1, B is a horizontal magnetic field with constant strength.

The governing equations on unsteady and laminar flow of electrically conducting fluid in the three-dimensional cylindrical coordinates (r, θ, z), by using the Boussinesq approximation, are expressed in the following. The continuity equation is as below,

$$\vec{\nabla}.\vec{V} = 0 \tag{1}$$

where $\vec{V}$ is the vector of velocity. The momentum equation is

$$(\vec{V}.\vec{\nabla})\vec{V} = -\frac{1}{\rho}\vec{\nabla}p + \nu\vec{\nabla}^2\vec{V} + \vec{g} + \vec{F} \tag{2}$$

in which t, p, ρ and ν are respectively time, pressure, density and kinematic viscosity. $\vec{g}$ is the vector of gravity and $\vec{F}$ is Lorentz force. Energy equation is expressed in the form of Eq. (3) by neglecting the viscous and ohmic dissipations.

$$(\vec{V}.\vec{\nabla})T = \alpha\vec{\nabla}^2 T \tag{3}$$

T is temperature and α is the thermal diffusion. Electric potential equation is as following:

$$\nabla^2\varphi = \vec{\nabla}.\left(\vec{V}\times\vec{B}\right) = \vec{V}.\left(\vec{\nabla}\times\vec{B}\right) + \vec{B}.\left(\vec{\nabla}\times\vec{V}\right) \tag{4}$$

in which $\vec{B}$ is the vector of magnetic field. Since the constant magnetic field is considered in this study, the term of $\vec{V}.(\vec{\nabla}\times\vec{B})$ becomes zero.

Electric current density, Lorentz force and the induced electric field, are obtained by Eq. (5):

$$\vec{J} = \sigma\left(\vec{E} + \vec{V}\times\vec{B}\right), \quad \vec{E} = -\vec{\nabla}\varphi \text{ and } \vec{F} = \vec{J}\times\vec{B} \tag{5}$$

where $\vec{J}$, σ and φ are respectively electric current density, fluid electrical conductivity and electric potential. Moreover, E and F are respectively induced electric field and the Lorentz force. The governing equations could be non-dimensional employing the following parameters:

$$\begin{aligned} &U = \frac{uD}{\alpha},\ V = \frac{vD}{\alpha},\ W = \frac{wD}{\alpha},\ R = \frac{r}{D},\ Z = \frac{z}{H},\ A = \frac{H}{D} \\ &P = \frac{pD^2}{\rho\alpha^2},\ T^* = \frac{T - T_c}{T_h - T_c},\ \Phi = \frac{\varphi}{B\alpha},\ E^* = \frac{ED}{B\alpha},\ F^* = \frac{FD}{\sigma B^2\alpha} \end{aligned} \tag{6}$$

where D is the characteristic length and is equal to (r_o-r_i). Substituting these parameters in Eqs. (1)–(4) gives the dimensionless form of the governing equations. Dimensionless continuity equation is obtained as

$$\frac{\partial U}{\partial R} + \frac{1}{R}\frac{\partial V}{\partial\theta} + \frac{1}{A}\frac{\partial W}{\partial Z} = 0 \tag{7}$$

Dimensionless momentum equations are as follows.

r component:

$$\begin{aligned} &U\frac{\partial U}{\partial R} + \frac{V}{R}\frac{\partial U}{\partial\theta} - \frac{V^2}{R} + \frac{1}{A}W\frac{\partial U}{\partial Z} = -\frac{\partial P}{\partial R} \\ &+\mathrm{Pr}\left[\frac{\partial^2 U}{\partial R^2} + \frac{1}{R}\frac{\partial U}{\partial R} + \frac{1}{R^2}\frac{\partial^2 U}{\partial\theta^2} + \frac{1}{A^2}\frac{\partial^2 U}{\partial Z^2} - \frac{U}{R^2} - \frac{2}{R^2}\frac{\partial V}{\partial\theta}\right] \\ &+Ha^2.\mathrm{Pr}\left[-\frac{\partial\Phi}{\partial Z}Cos\theta - UCos^2\theta + \frac{1}{2}VSin2\theta\right] \end{aligned} \tag{8}$$

θ component:

$$\begin{aligned} &U\frac{\partial V}{\partial R} + \frac{V}{R}\frac{\partial V}{\partial\theta} + \frac{UV}{R} + \frac{1}{A}W\frac{\partial V}{\partial Z} = -\frac{1}{R}\frac{\partial P}{\partial\theta} \\ &+\mathrm{Pr}\left[\frac{\partial^2 V}{\partial R^2} + \frac{1}{R^2}\frac{\partial^2 V}{\partial\theta^2} + \frac{1}{R}\frac{\partial V}{\partial R} + \frac{1}{A^2}\frac{\partial^2 V}{\partial Z^2} - \frac{V}{R^2} + \frac{2}{R^2}\frac{\partial U}{\partial\theta}\right] \\ &+Ha^2.\mathrm{Pr}\left[\frac{\partial\Phi}{\partial Z}Sin\theta + \frac{1}{2}USin2\theta - VSin^2\theta\right] \end{aligned} \tag{9}$$

z component:

$$U\frac{\partial W}{\partial R}+\frac{V}{R}\frac{\partial W}{\partial \theta}+\frac{1}{A}W\frac{\partial W}{\partial Z}=-\frac{1}{A}\frac{\partial P}{\partial Z}+\Pr\left[\frac{\partial^2 W}{\partial R^2}+\frac{1}{R^2}\frac{\partial^2 W}{\partial \theta^2}+\frac{1}{R}\frac{\partial W}{\partial R}+\frac{1}{A^2}\frac{\partial^2 W}{\partial Z^2}\right]$$
$$+Ra.\Pr.T^*+Ha^2.\Pr\left[\frac{\partial \Phi}{\partial R}Cos\theta-\frac{1}{R}\frac{\partial \Phi}{\partial \theta}Sin\theta-WSin^2\theta+WCos^2\theta\right] \quad (10)$$

Dimensionless energy equation and dimensionless electric potential equation are indicated in Eqs. (11) and (12) respectively:

$$U\frac{\partial T^*}{\partial R}+\frac{V}{R}\frac{\partial T^*}{\partial \theta}+\frac{1}{A}W\frac{\partial T^*}{\partial Z}=\frac{\partial^2 T^*}{\partial R^2}+\frac{1}{R^2}\frac{\partial^2 T^*}{\partial \theta^2}+\frac{1}{R}\frac{\partial T^*}{\partial R}+\frac{1}{A^2}\frac{\partial^2 T^*}{\partial Z^2} \quad (11)$$

$$\frac{\partial^2 \Phi}{\partial R^2}+\frac{1}{R^2}\frac{\partial^2 \Phi}{\partial \theta^2}+\frac{1}{R}\frac{\partial \Phi}{\partial R}+\frac{\partial^2 \Phi}{\partial Z^2}=$$
$$\frac{\partial W}{\partial R}Cos\theta+\frac{1}{r}WCos\theta-\frac{1}{R}\frac{\partial W}{\partial \theta}Sin\theta+\frac{1}{A}\frac{\partial V}{\partial Z}Sin\theta-\frac{1}{A}\frac{\partial U}{\partial Z}Cos\theta \quad (12)$$

where, *Ra* and Pr are defined as follows:

$$Ra=\frac{g\beta(T_H-T_C)D^3}{\upsilon\alpha},\ \Pr=\frac{\upsilon}{\alpha} \quad (13)$$

The effect of the magnetic field is introduced into the momentum and potential equations through the Hartmann number. The Hartmann number is known as:

$$Ha=BD\sqrt{\frac{\sigma}{\mu}} \quad (14)$$

The local and average Nusselt numbers along the inner cylinder are defined as follows:

$$Nu\ (\theta,Z)=\left.\frac{\partial T^*}{\partial R}\right|_{R=R_i},\quad \overline{Nu}=\frac{1}{2\pi}\int_0^{2\pi}\int_0^{A}Nu\ (\theta,Z)\,dZd\theta \quad (15)$$

where *A* is the aspect ratio and is equal to *H/D*.

Regarding the boundary and initial conditions, velocities are assumed zero on all walls based on No-slip conditions. Constant temperatures at outer ($T_o^*=0$) and the inner ($T_i^*=1$) cylindrical walls are considered. Adiabatic conditions are assumed at the top and bottom walls ($\partial T^*/\partial Z=0$). All walls are also presumed to be electrically insulated ($\partial \Phi/\partial n=0$). Moreover, τ, T^*, *U*, *V* and *W* are assumed zero at initial time.

3. Numerical procedure

To attain the velocity field Lorentz force, mass and momentum conservation equations should be solved. Then, Eqs. (11) and (12) must be solved by substituting the velocity field obtained in the previous step. After that, the distributions of temperature and electric potential are calculated that lead to obtain the electric current density by Eq. (5). Finally, Lorentz force and buoyancy force could be determined and replaced again in momentum equation.

As we know, complex nonlinear governing equations should be solved numerically by means of the finite volume method (FV). The central difference method is used for discretizing diffusion terms. The use of this method for convective terms causes divergence or unrealistic answers in some cases. Therefore, hybrid approach is used to discretize the convection terms that combines central difference and upstream methods. A staggered grid system, in which the velocity components are stored midway between the scalar storage locations, is used. In order to couple the pressure and velocity field in the momentum equations, the SIMPLER algorithm is approved for solving the coupled equations [26].

4. Grid independency and results verification

4.1. Grid independency

In order to obtain a grid-independent solution, different grids were studied and the optimal grid was selected. To this end, a case with expected maximum temperature gradients and velocities was selected, on which the mesh-independency analysis was carried out. Hence, an annulus with A = 1, $\lambda=2$ and Pr = 0.072 was evaluated in the absence of magnetic field. Initially, attempts were made to determine the optimal number of meshes for the grid in directions *r*, θ, and *z*, respectively represented by N_r, N_θ, and N_z (see Fig. 2). After determining the optimal number of meshes in the grid for different directions, the dimensionless axial velocity (W) as well as the dimensionless temperature (T*) on the line of symmetry of the annulus (Z = A/2) were compared for three different grids. As shown in Fig. 3, the difference in the results of $40\times60\times40$ and

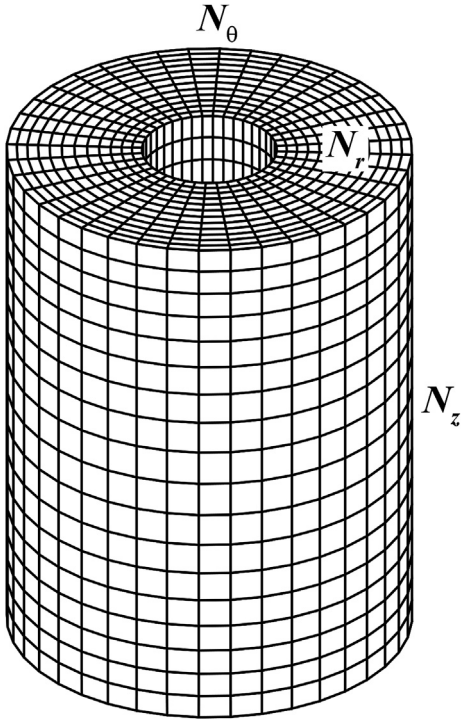

Fig. 2. An adapted structured grid on the annulus.

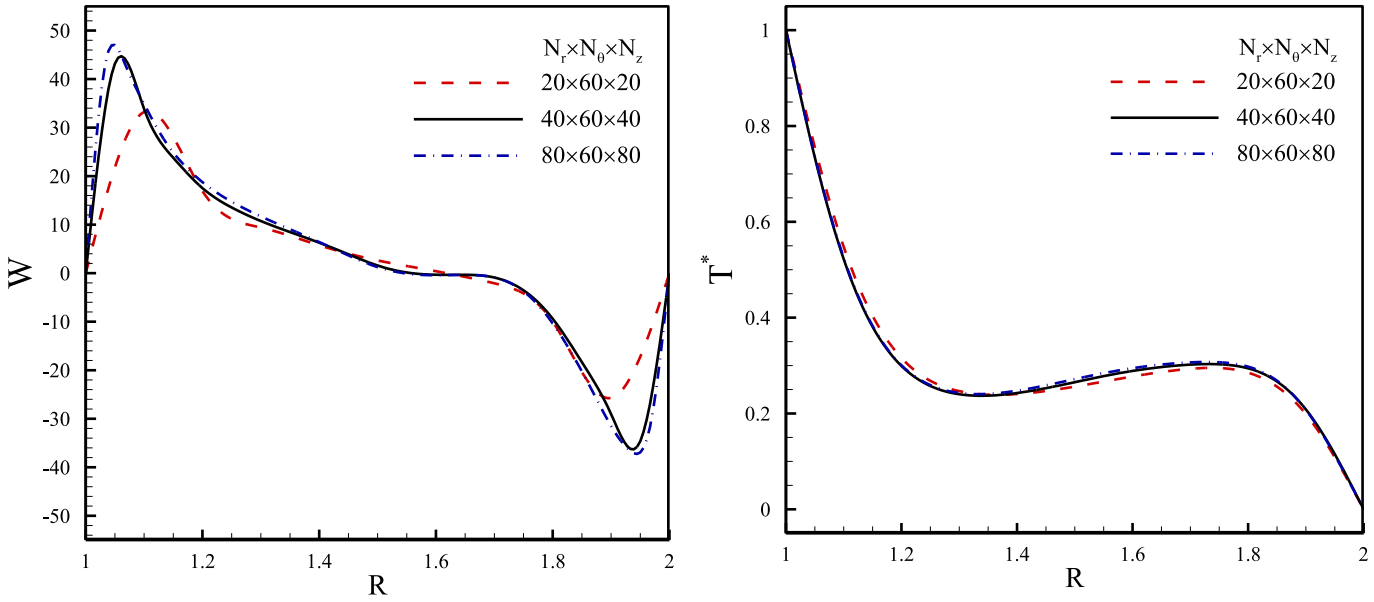

Fig. 3. Profiles of dimensionless axial velocity (left) and dimensionless temperature (right) for different grids (A = 1, $\lambda = 2$ and Pr = 0.072).

$80 \times 60 \times 80$ are negligible, and, hence, the grid of $40 \times 60 \times 40$ was decided as appropriate for this model. For further calculations in other models, appropriate grids with respect to the dimensions were used.

4.2. Results verification

In order to verify the performance of the computer code, the derived governing equations for 3-dimensional cases were simulated and applied on some sample problems, and then the results were compared to the previously available data. First, natural convection in the annulus with constant temperature horizontal walls and insulated vertical walls was compared to the experimental study of Wrobel et al. [20]. In this comparison, natural convection of a fluid with a Prandtl number of 61 in an annulus with an outer to inner diameter ratio of 2.7 and an aspect ratio of 5.41 was investigated. The results of this comparison are presented in Fig. 4 for average Nusselt number. According to the results, the maximum difference was smaller than 8%, which is considered negligible for an experimental study, indicating a good agreement between the results.

For a more accurate study of the results, the results of the present study for a fluid with a Prandtl number of 0.7 in a annulus with an outer to inner diameter ratio of 2 and an aspect ratio of 1 were compared with the numerical results reported in Refs. [19] and [27]. The comparison was made for a wide range of Rayleigh numbers, the results of which are given in Fig. 5. As shown, the results are in good agreement with an error of lower than 2%.

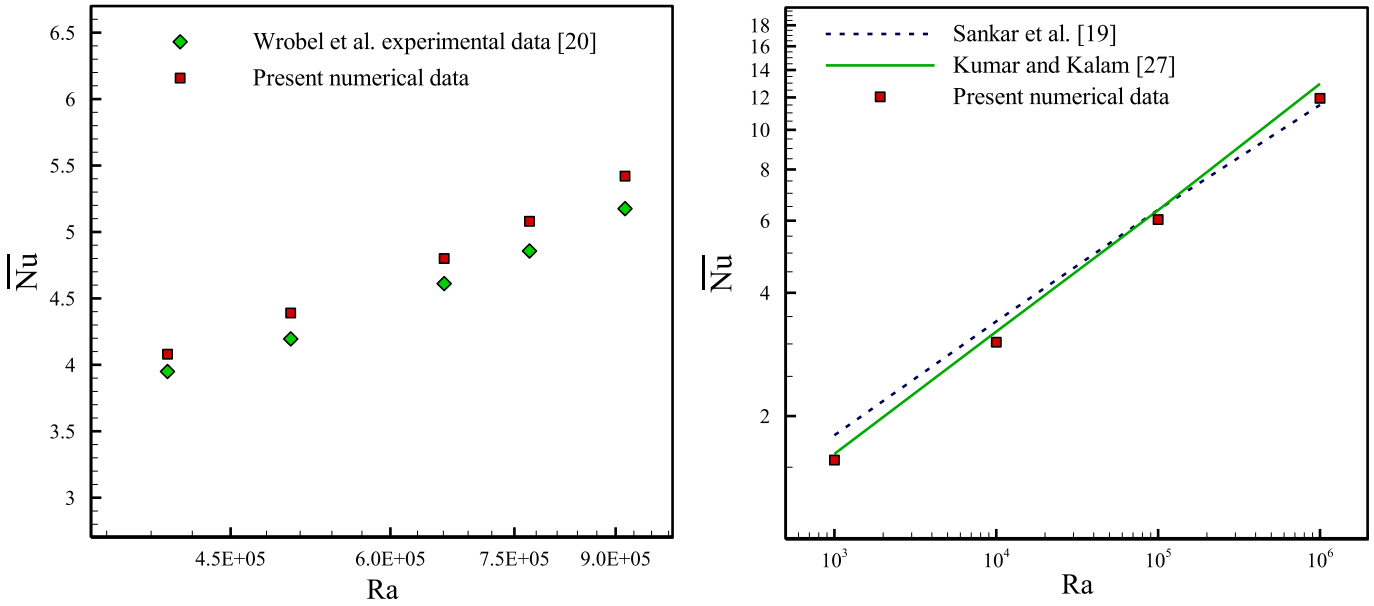

Fig. 4. Comparison of average Nusselt number results with previous experimental (left) and numerical data (right).

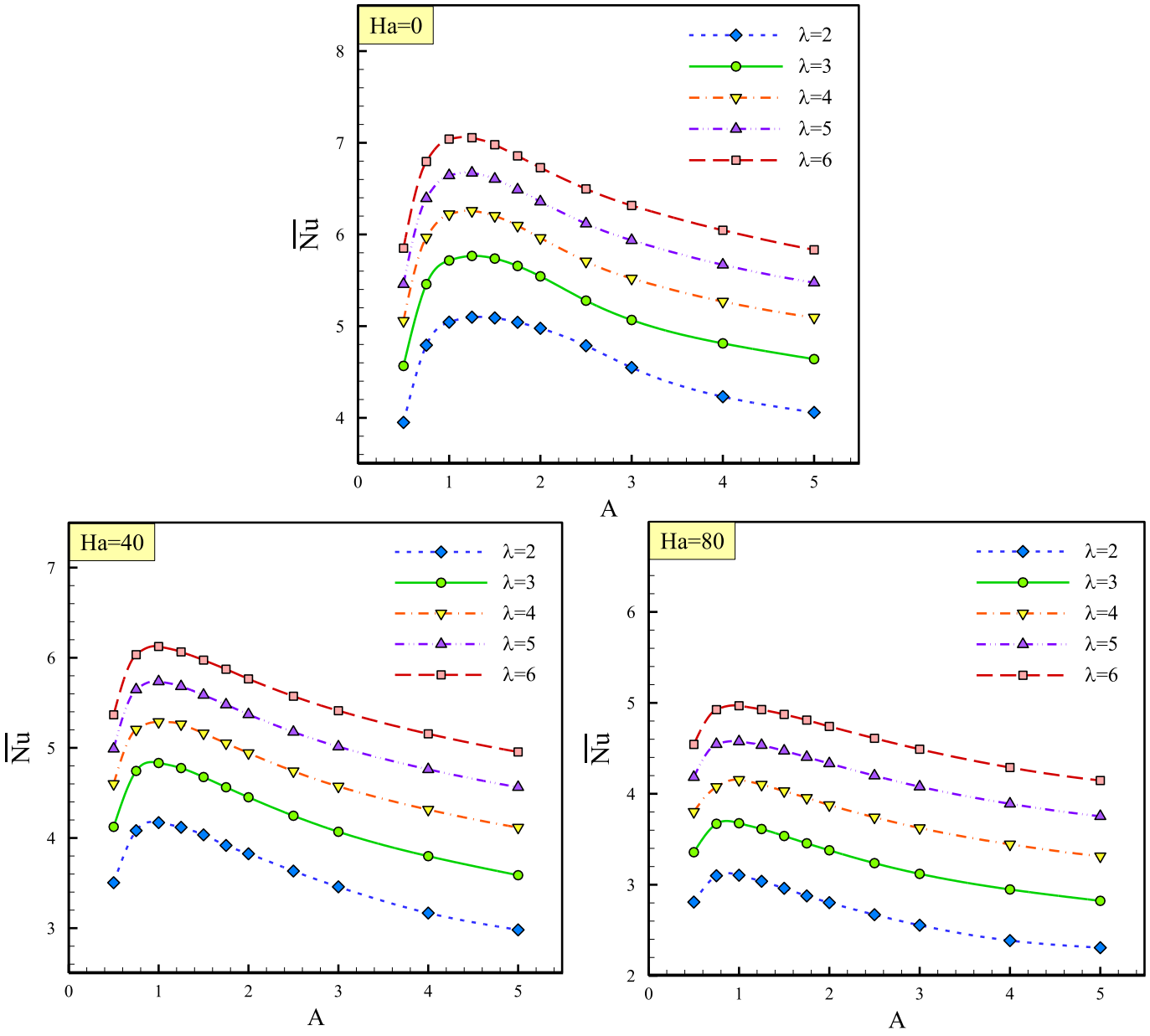

Fig. 5. Average Nusselt number versus aspect ratios for various aspect ratio and Hartman numbers. (Ra=105 and Pr=0.072).

5. Results and discussion

5.1. Effects of Hartman number, aspect ratio and radii ratio on average Nusselt number

Figs. 5 and 6 show respectively the effects of aspect ratio and radii ratio on the average Nusselt number for Pr = 0.072 and Ra = 10^5. As observed in Fig. 5, there are two different trends at all Hartmann numbers and aspect ratios. For aspect ratios lower than about 1, an increase in the height of the annulus results in a higher average Nusselt number. The reason may be related to a more effective flow pattern for heat transfer. This trend has previously been reported by Newell and Schmidt [28] and Kuehn and Goldstein [29]. When aspect ratio is greater than about 1, the average Nusselt number decreases as A is enlarged. This is due to the fact that most of the heat transfer into the fluid arises close to the bottom of the hot wall. This phenomenon can be seen in the graphs of local Nusselt number presented by Afrand et al. [16]. Therefore, increasing the height of the cylindrical annulus leads to a reduction in the total heat transfer rate and consequently the average Nusselt number decreases. The results of Newell and Schmidt [28] and Wilkes and Churchill [30] also show this trend.

The effect of radii ratio on the average Nusselt number for cylindrical annulus with aspect ratios of 0.5, 1 and 3 is shown in Fig. 6. It can be seen that with increasing radii ratio (λ) the average Nusselt number significantly augments at all Hartman numbers and aspect ratios. This can be related to the temperature and velocity fields in the fluid. Since increasing the radii ratio leads to an increase in the curvature of the inner wall, fluid flow has less area to move near the inner wall. Thus, the fluid velocity increases to reach the mass conservation equation. This increase in the velocity can reduce the thickness of the thermal boundary layer and accordingly the average Nusselt number increases. The results correspond to radii ratio effect on the average Nusselt number follow the same trend as

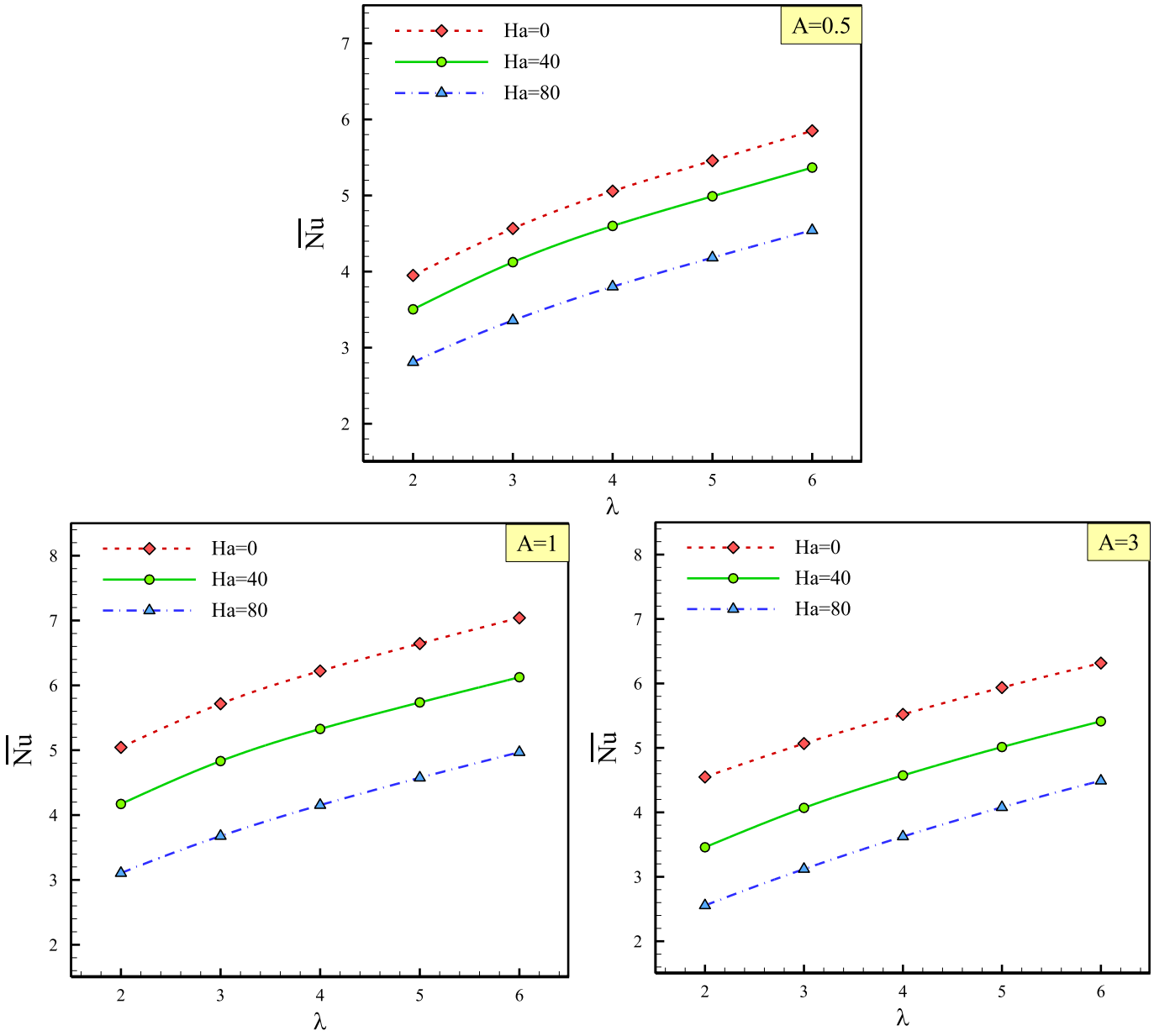

Fig. 6. Average Nusselt number versus radii ratio for various aspect ratio and Hartman numbers. (Ra = 105 and Pr = 0.072).

reported by Prasad and Kulacki [31] and Satya Sai et al. [32].

It is evident from Figs. 5 and 6 that with increasing Hartmann number, the trends are also observed with a lower slope. In fact, the magnetic field suppresses the natural convection of the fluid that is discussed in detail in the following sections.

5.2. Evaluation of distribution of temperature, Lorentz force and induced electric field

The distribution of temperature, Lorentz force and induced electric field in different vertical and horizontal plane in the presence and absence of magnetic field are depicted in Figs. 7 and 8. As is evident in Fig. 7, the induced electric field is zero in the x-plane and is maximized in the y-plane. In fact, the magnetic field is perpendicular to term of $\nabla \times \vec{V}$ in the x-plane due to the axisymmetric flow in this model; thus, the electric potential is zero in this plane based on Eq. (4). However, it can be seen in Fig. 7 that the Lorentz force is maximized in the x-plane and that it is minimal in the y-plane. Based on Eq. (5), the is composed of two factors: $\vec{E}$ and $\vec{V} \times \vec{B}$. It is found from Eq. (5) and Fig. 6 that in regions where the terms of $\vec{E}$ and $\vec{V} \times \vec{B}$ are equal to each other the electric current density is zero, resulting in zero Lorentz force. In other regions, it is possible that the term of $\vec{V} \times \vec{B}$ win against $\vec{E}$, or vice versa. In both cases the Lorentz force is generated opposed to the direction of flow.

The effect of the magnetic field on the isotherms also is presented in Fig. 7. The isotherms are close to each other in the absence of magnetic field (Ha = 0) indicating that there is a considerable temperature gradient near the walls. It can be observed that by increasing Hartman number up to 80 the temperature stratification exists in the x-plane, while it is not observed in the y-plane. This is because of an increase in Lorentz force (especially in x-plane) that prevents the movement of fluid. This means that the values of Lorentz force in the x-plane is more than that in y-plane, which is

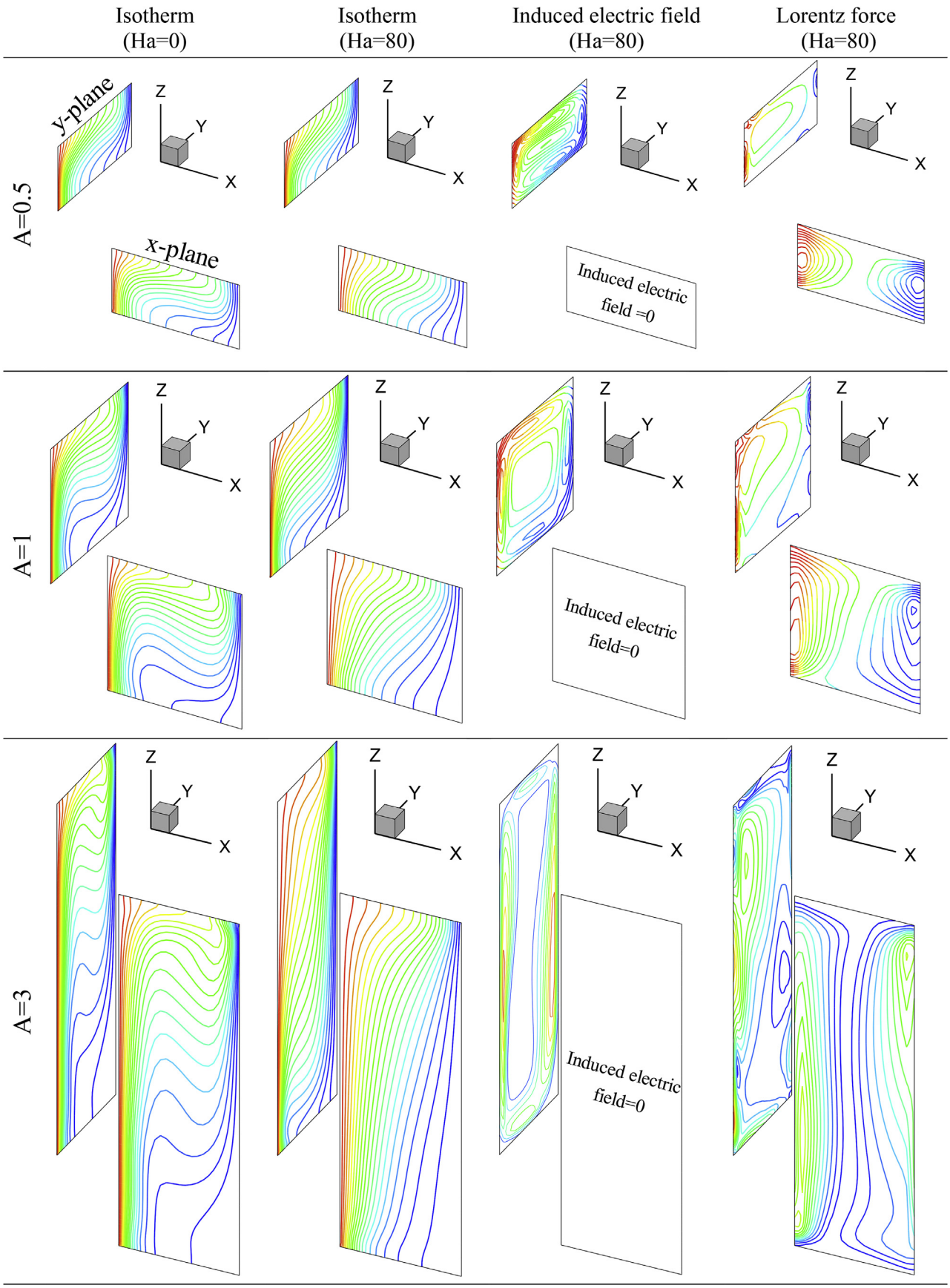

Fig. 7. Distribution of temperature, Lorentz force and induced electric field in the vertical planes in the presence and absence of magnetic field (Ra = 10^5, λ = 2 and Pr = 0.072).

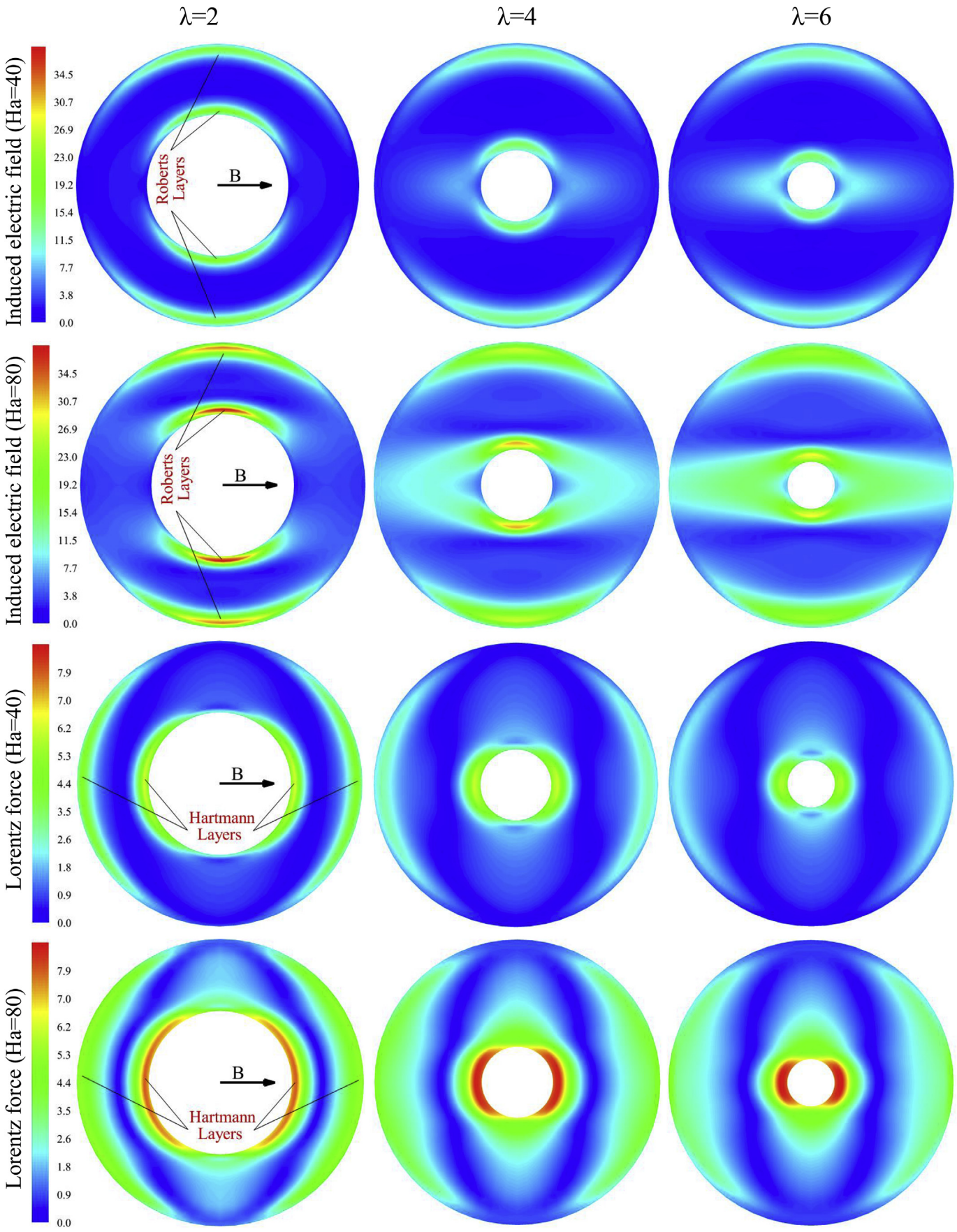

Fig. 8. Induced electric field and Lorentz force distribution and in the horizontal plane (Z = 0.5). (Ra = 10^5, A = 1 and Pr = 0.072).

confirmed by distribution of Lorentz force in Fig. 7. A comparison between isotherms in x-plane with that in y-plane also reveals that magnetic field creates the electric potential (especially in y-plane) that leads to reduce the Lorentz force against buoyancy force. This is in good agreement with the contours correspond to distribution of Lorentz force and induced electric field in Fig. 7. These phenomena are observed for all aspect ratios.

The distribution of the Lorentz force and induced electric field in the central horizontal plane of the annulus for various Hartmann numbers and radii ratios are depicted in Fig. 8. Hartmann layers and Roberts layers are marked in this figure. By comparing Fig. 8 with Fig. 7, it is found that the Lorentz force in the Hartmann layer is much superior, while the induced electric field in the Roberts layer has more value.

In both Figs. 7 and 8, it is obvious that the horizontal magnetic field causes a lack of symmetry. This phenomenon happens due to the Roberts layers and Hartmann layers develop near the walls parallel and perpendicular to the horizontal magnetic field [33,34]. As previously mentioned, the Lorentz force is maximum where the magnetic field would be perpendicular to the wall (x-plane); thus, it can be concluded that Hartmann layer thickness is related to $(\mathrm{Cos}\theta)^{-1}$. Moreover, as shown in this figure, with increasing Hartmann number the values of Lorentz force and induced electric field strongly increase.

In fact, the influence of Hartmann and Roberts layers on the flow can be expressed using the Lorentz force, which tends to resist movement of the fluid. It can be found from Eq. (5) that the Lorentz force is a resistance force against the flow and it is more powerful where the velocity is greater. As we know, the fluid near the walls has a higher velocity compared to other regions of the annulus. Accordingly, the Lorentz force is higher near the walls that perpendicular to the magnetic field, resulting in formation of Hartmann layer. Since the radial velocity is perpendicular to the magnetic field in y-plane, based on Eq. (5), the Lorentz force in y-plane is very small. It causes the Hartmann layer does not appear in this plane. The same phenomenon occurs in the opposite plane for induced electric field. In fact, there is a much steeper velocity gradient near the walls of than other regions of the annulus. In the y-plane, the term of $\vec{\nabla} \times \vec{V}$ and $\vec{B}$ are parallel, resulting in greater induced electric field and Roberts layer.

By inspecting Fig. 8, it is understood that with increasing radii ratio the Lorentz force increases and induced electric field decreases. As previously mentioned, increasing the radii ratio leads to an increase in velocity, resulting in higher Lorentz force.

5.3. Effects of Prandtl and Hartman numbers

Fig. 9 shows the impact of Prandtl and Hartmann numbers on the average Nusselt number for annuluses with radii ratios of 2 and 6. As observed in this figure, the average Nusselt number increases with increasing Prandtl number at all Hartmann numbers. In fact, with growing the Prandtl number, viscous force augments and thermal diffusivity decreases. In addition, it is expected that with increasing Prandtl number, the thickness of momentum boundary layer increases, while the thickness of thermal boundary layer decreases. It is clear that the temperature gradient can be increased by reducing the thickness of the thermal boundary layer, resulting in higher average Nusselt number. As shown in this figure, for different Prandtl numbers, the effect of Hartmann number on the average Nusselt number is almost similar. It is also found from this figure that with increasing Hartmann number, the effect of Prandtl number on the average Nusselt number decreases. The reason is related to this fact that at higher Hartmann number the convective heat transfer is suppressed by the Lorentz force and thus the impact of boundary layers decreases.

Another point that can be understood from this figure is that the average Nusselt number decreases with increasing Hartmann number for all radii ratios and Prandtl numbers. As mentioned earlier, the Lorentz force can suppress the convictive heat transfer. Thus, it is expected when the Lorentz force increases excessively, heat transfer converts to conduction mode. In this situation, the expectation is that the average Nusselt number along the inner cylinder approaches the asymptotic value of $Nu_{i,cond}$ that is defined as follows [13]:

$$Nu_{i,cond} = \frac{(\lambda - 1)}{\ln(\lambda)} \tag{16}$$

For example, for case of $\lambda = 2$ and $\lambda = 6$, the average Nusselt number must respectively be equal to 1.44 and 2.79 in accordance

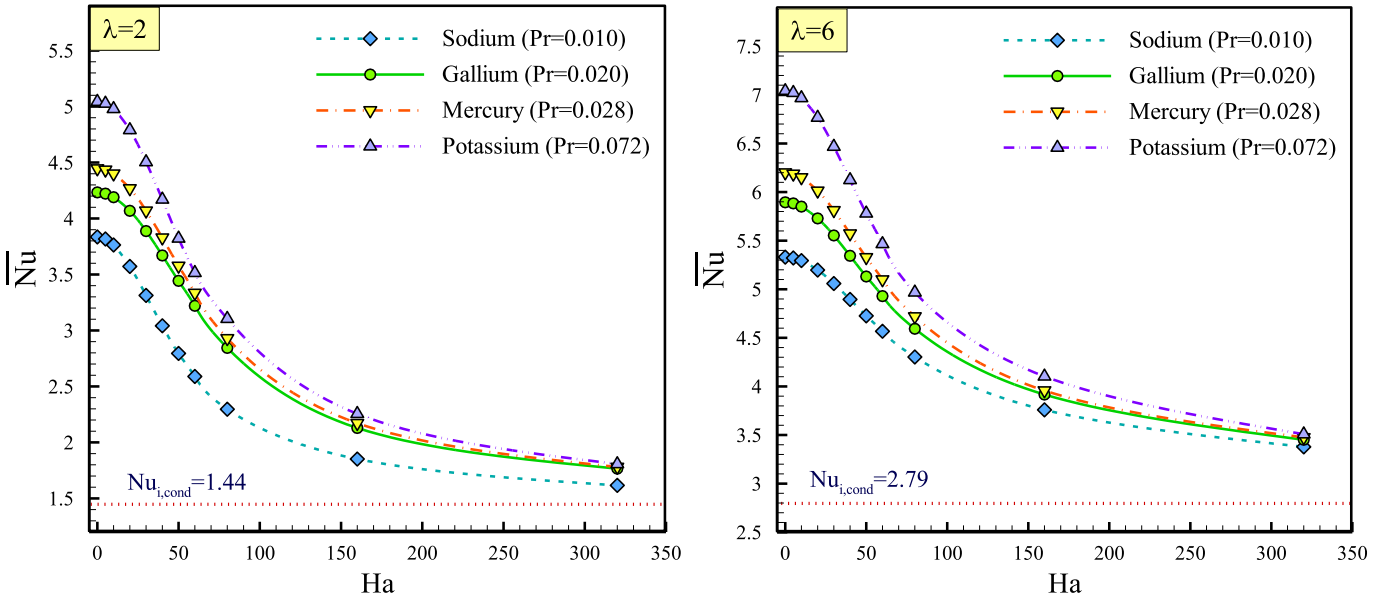

Fig. 9. Impact of Prandtl and Hartmann numbers on the average Nusselt number for annuluses with radii ratios of 2 and 6 (Ra = 105, A = 1).

with Eq. (16). Tend to the asymptotic values of $Nu_{i,cond}$ is evident in Fig. 9. However, it can be observed that in the case of $\lambda = 2$ pure conduction achievable at Ha~320, while it is possible at Hartmann numbers higher than 320. It can be concluded that a stronger magnetic field is needed to achieve pure conduction in the case of thick annulus (e.g. $\lambda = 6$).

5.4. Inspecting the effect of magnetic field strength on average Nusselt number

To better understand the effect of magnetic field strength on natural convection, 3D graphs of the average Nusselt number versus Hartmann number and aspect ratio for annuluses with radii ratios of 2, 4 and 6 are displayed in Fig. 10. It is clearly evident that for different radii ratios, the effect of Hartmann number and aspect ratio on the average Nusselt number is almost similar. It is also observed that the behavior of average Nusselt number that was expressed as a function of the aspect ratio, mentioned in, can be observed for all Hartmann numbers Furthermore, the average Nusselt number decreases as Hartmann number is increased. As mentioned in subsection 5.2, the effects of $\vec{E}$ and $\vec{V} \times \vec{B}$ on the electric current density are exactly opposite. However, the Lorentz force is generated opposed to the direction of flow and consequently reduces the average Nusselt number.

6. Conclusion

In the present study, laminar natural convection in a vertical cylindrical annulus containing various electrically conductive fluids under a horizontal magnetic field was studied. The annulus was composed of two isothermal coaxial cylinders. Both ends of the cylinders were supposed adiabatic and all walls were assumed electrically insulated. The effects of different parameters such as Hartman number, the radii ratio, aspect ratio, and Prandtl number on the temperature distribution, average Nusselt number, distribution of Lorentz forces as well as induced electric field were investigated. The main results of this study are as follows:

- For aspect ratios lower than about 1, an increase in the aspect ratio resulted in a higher average Nusselt number. When aspect ratio was greater than about 1, the average Nusselt number decreases as aspect ratio was enlarged.
- A stronger magnetic field is needed to achieve pure conduction in the case of thick annulus (e.g. $\lambda = 6$).
- Results also revealed that a stronger magnetic field was needed to achieve pure conduction in the case of thick annulus. The presence of magnetic field led to the induction of electric field which affected the Lorentz force.

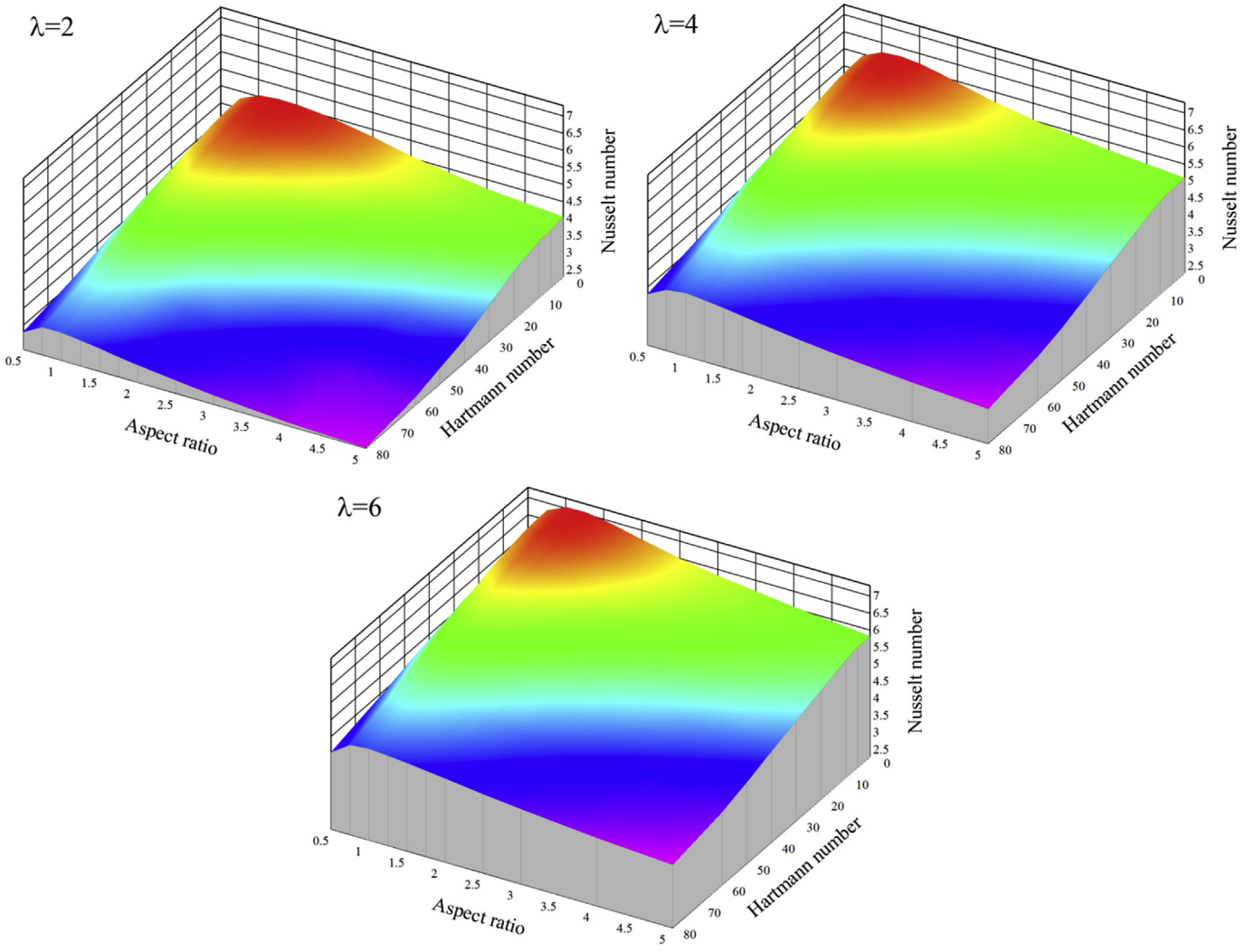

Fig. 10. 3D graphs of the average Nusselt number versus Hartmann number and aspect ratio for annuluses with radii ratios of 2, 4 and 6 ($Ra = 10^5$, $Pr = 0.072$).

- Distributions of Lorentz force and induced electric field indicated respectively the formation of Hartmann and Roberts layers. The Lorentz force was much greater in the Hartmann layer, while the induced electric field had more value in the Roberts layer.
- The average Nusselt number increased with increasing Prandtl number at all Hartmann numbers. With increasing Hartmann number, the effect of Prandtl number on the average Nusselt number decreased.
- When the Lorentz force increases excessively, heat transfer converts to conduction mode. In this situation, the average Nusselt number along the inner cylinder approaches the asymptotic value of $Nu_{i,cond}$.

Acknowledgments

The author is grateful to Najafabad Branch, Islamic Azad University, Najafabad, Iran for the support.

References

[1] Malvandi DDGanji. Brownian motion and thermophoresis effects on slip flow of alumina/water nanofluid inside a circular microchannel in the presence of a magnetic field. Int J Therm Sci 2014;84:196–206.
[2] Teamah MA, El-Maghlany WM. Augmentation of natural convective heat transfer in square cavity by utilizing nanofluids in the presence of magnetic field and uniform heat generation/absorption. Int J Therm Sci 2012;58:130–42.
[3] Hemmat Esfe M, Saedodin S, Sina N, Afrand M, Rostami S. Designing an artificial neural network to predict thermal conductivity and dynamic viscosity of ferromagnetic nanofluid. Int Commun Heat Mass Transf 2015;68:50–7.
[4] Afrand M, Toghraie D, Ruhani B. Effects of temperature and nanoparticles concentration on rheological behavior of Fe3O4–Ag/EG hybrid nanofluid: an experimental study. Exp Therm Fluid Sci 2016;77:38–44.
[5] Afrand M, Toghraie D, Sina N. Experimental study on thermal conductivity of water-based Fe3O4 nanofluid: development of a new correlation and modeled by artificial neural network. Int Commun Heat Mass Transf 2016;75:262–9.
[6] Toghraie D, Alempour SM, Afrand M. Experimental determination of viscosity of water based magnetite nanofluid for application in heating and cooling systems. J Magn Magn Mater 2016;417:243–8.
[7] Abdollahi A, Reza Salimpour M. Experimental investigation on the boiling heat transfer of nanofluids on a flat plate in the presence of a magnetic field. Eur Phys J Plus 2016;131:414.
[8] Goharkhah M, Ashjaee M, Shahabadi M. Experimental investigation on convective heat transfer and hydrodynamic characteristics of magnetite nanofluid under the influence of an alternating magnetic field. Int J Therm Sci 2016;99:113–24.
[9] Kasaeipoor A, Ghasemi B, Aminossadati SM. Convection of Cu-water nanofluid in a vented T-shaped cavity in the presence of magnetic field. Int J Therm Sci 2015;94:50–60.
[10] Ghasemi B, Aminossadati SM, Raisi A. Magnetic field effect on natural convection in a nanofluid-filled square enclosure. Int J Therm Sci 2011;50:1748–56.
[11] Kefayati GR. FDLBM simulation of mixed convection in a lid-driven cavity filled with non-Newtonian nanofluid in the presence of magnetic field. Int J Therm Sci 2015;95:29–46.
[12] Mahmoodi M, Esfe MH, Akbari M, Karimipour A, Afrand M. Magneto-natural convection in square cavities with a source-sink pair on different walls. Int J Appl Electromagn Mech 2015;47:21–32.
[13] Afrand M, Farahat S, Nezhad AH, Sheikhzadeh GA, Sarhaddi F. Numerical simulation of electrically conducting fluid flow and free convective heat transfer in an annulus on applying a magnetic field. Heat Transf Res 2014;45:749–66.
[14] Afrand M, Farahat S, Nezhad AH, Sheikhzadeh GA, Sarhaddi F, Wongwises S. Multi-objective optimization of natural convection in a cylindrical annulus mold under magnetic field using particle swarm algorithm. Int Commun Heat Mass Transf 2015;60:13–20.
[15] Kakarantzas S, Sarris I, Vlachos N. Natural convection of liquid metal in a vertical annulus with lateral and volumetric heating in the presence of a horizontal magnetic field. Int J Heat Mass Transf 2011;54:3347–56.
[16] Afrand M, Rostami S, Akbari M, Wongwises S, Esfe MH, Karimipour A. Effect of induced electric field on magneto-natural convection in a vertical cylindrical annulus filled with liquid potassium. Int J Heat Mass Transf 2015;90:418–26.
[17] Mozayyeni H, Rahimi A. Mixed convection in cylindrical annulus with rotating outer cylinder and constant magnetic field with an effect in the radial direction. Sci Iran 2012;19:91–105.
[18] Teimouri H, Afrand M, Sina N, Karimipour A, Isfahani AHM. Natural convection of liquid metal in a horizontal cylindrical annulus under radial magnetic field. Int J Appl Electromagn Mech 2015;49:453–61.
[19] Sankar M, Venkatachalappa M, Shivakumara I. Effect of magnetic field on natural convection in a vertical cylindrical annulus. Int J Eng Sci 2006;44:1556–70.
[20] Wrobel W, Fornalik-Wajs E, Szmyd J. Experimental and numerical analysis of thermo-magnetic convection in a vertical annular enclosure. Int J Heat Fluid Flow 2010;31:1019–31.
[21] El-Kabeir S, El-Hakiem M, Rashad A. Group method analysis of combined heat and mass transfer by MHD non-Darcy non-Newtonian natural convection adjacent to horizontal cylinder in a saturated porous medium. Appl Math Model 2008;32:2378–95.
[22] Venkatachalappa M, Do Y, Sankar M. Effect of magnetic field on the heat and mass transfer in a vertical annulus. Int J Eng Sci 2011;49:262–78.
[23] Kumar A, Singh A. Effect of induced magnetic field on natural convection in vertical concentric annuli heated/cooled asymmetrically. J Appl Fluid Mech 2013;6:15–26.
[24] Afrand M, Farahat S, Nezhad AH, Ali Sheikhzadeh G, Sarhaddi F. 3-D numerical investigation of natural convection in a tilted cylindrical annulus containing molten potassium and controlling it using various magnetic fields. Int J Appl Electromagn Mech 2014;46:809–21.
[25] Afrand M, Sina N, Teimouri H, Mazaheri A, Safaei MR, Esfe MH, et al. Effect of magnetic field on free convection in inclined cylindrical annulus containing molten potassium. Int J Appl Mech 2015;7:1550052.
[26] Patankar S. Numerical heat transfer and fluid flow. CRC press; 1980.
[27] Kumar R, Kalam M. Laminar thermal convection between vertical coaxial isothermal cylinders. Int J Heat Mass Transf 1991;34:513–24.
[28] Newell M, Schmidt F. Heat transfer by laminar natural convection within rectangular enclosures. J Heat Transf 1970;92:159–67.
[29] Kuehn T, Goldstein R. An experimental and theoretical study of natural convection in the annulus between horizontal concentric cylinders. J Fluid Mech 1976;74:695–719.
[30] Wilkes J, Churchill S. The finite-difference computation of natural convection in a rectangular enclosure. AIChE J 1966;12:161–6.
[31] Prasad V, Kulacki F. Natural convection in a vertical porous annulus. Int J Heat Mass Transf 1984;27:207–19.
[32] Satya Sai B, Seetharamu K, Aswatha Narayana P, Reddy J. Finite element analysis of the effect of radius ratio on natural convection in an annular cavity. Int J Numer Methods Heat Fluid Flow 1993;3:305–18.
[33] Todd L. Hartmann flow in an annular channel. J Fluid Mech 1967;28:371–84.
[34] Kakarantzas S, Grecos A, Vlachos N, Sarris I, Knaepen B, Carati D. Direct numerical simulation of a heat removal configuration for fusion blankets. Energy Convers Manag 2007;48:2775–83.